SIMULATION OF PHYSICAL PROCESSES

Conference materials
UDC 539.1.072+615.849.5
DOI: https://doi.org/10.18721/JPM.184.114

Nanoparticle size and quantity impact on X-ray induced secondary emission for magnetite-gold systems

N.S. Markin [1, 2] ✉, I.S. Gordeev [3, 4], S.I. Ivannikov [2],
A.Yu. Samardak [1], A.S. Samardak [1], A.V. Ognev [1]

[1] Far Eastern Federal University, Vladivostok, Russia;
[2] Institute of Chemistry FEB RAS, Vladivostok, Russia;
[3] Joint Institute for Nuclear Research, Dubna, Russia;
[4] Dubna State University, Dubna, Russia
✉ markkin.ns@gmail.com

Abstract. The work presents the results of Monte Carlo modeling (PHITS) of irradiation of Fe_3O_4-SiO_2-Au nanoparticles – promising agents for enhancing the effectiveness of radiation therapy with X-ray radiation. Within the model of a single nanoparticle in a water phantom, it was shown that, assuming a uniform distribution of gold nanoparticles over the surface of the adhesion layer, the particle density and their size do not have a significant impact on the efficiency of therapeutic X-ray beam conversion. The main factors determining the configuration of dose fields are the chemical composition of the nanoparticles and the energy of the primary photon beam.

Keywords: gold nanoparticles, Monte Carlo simulation, radiosensitizer, radiation therapy

Funding: The study of Markin N.S., Samardak A.Yu., Ognev A.V. was supported by the Russian Ministry of Science and Higher Education (State Task No. FZNS-2023-0012).

Citation: Markin N.S., Gordeev I.S., Ivannikov S.I., Samardak A.Yu., Samardak A.S., Ognev A.V., Nanoparticle size and quantity impact on X-ray induced secondary emission for magnetite-gold systems, St. Petersburg State Polytechnical University Journal. Physics and Mathematics. 18 (4.1) (2025) 87–92. DOI: https://doi.org/10.18721/JPM.184.114

Материалы конференции
УДК 539.1.072+615.849.5
DOI: https://doi.org/10.18721/JPM.184.114

Влияние размера и числа золотых наночастиц в системе магнетит-золото на эмиссию рентген-индуцированного вторичного излучения

Н.С. Маркин [1, 2] ✉, И.С. Гордеев [3, 4], С.И. Иванников [2],
А.Ю. Самардак [1], А.С. Самардак [1], А.В. Огнев [1]

[1] Дальневосточный федеральный университет, г. Владивосток, Россия;
[2] Институт химии ДВО РАН, г. Владивосток, Россия;
[3] Объединенный институт ядерных исследований, г. Дубна, Россия
[4] Государственный университет «Дубна», г. Дубна, Россия
✉ markkin.ns@gmail.com

Аннотация. В работе представлены результаты Монте-Карло моделирования (PHITS) облучения наночастицы состава Fe_3O_4-SiO_2-Au – перспективного агента для повышения

эффективности лучевой терапии – рентгеновским излучением. В рамках одночастичной модели наночастицы в водном фантоме показано, что при условии равномерного распределения наночастиц золота по поверхности адгезионного слоя плотность нанесения частиц и их размер не оказывают значимого воздействия на эффективность конверсии рентгеновского излучения. Основными факторами, определяющими конфигурацию дозовых полей, являются химический состав наночастиц и энергия первичного фотонного пучка.

Ключевые слова: золотые наночастицы, Монте-Карло моделирование, радиосенсибилизатор, лучевая терапия

Финансирование: Государственное задание Дальневосточного федерального университета No. FZNS-2023-0012.

Ссылка при цитировании: Маркин Н.С., Гордеев И.С., Иванников С.И., Самардак А.Ю., Самардак А.С., Огнев А.В. Влияние размера и числа золотых наночастиц в системе магнетит-золото на эмиссию рентген-индуцированного вторичного излучения // Научно-технические ведомости СПбГПУ. Физико-математические науки. 2025. Т. 18. № 4.1. С. 87–92. DOI: https://doi.org/10.18721/JPM.184.114

Introduction

One of the main limitations of X-ray radiotherapy is the lack of selectivity of ionizing radiation action on the tumor, which leads to increased risks of unwanted irradiation of healthy tissues and, consequently, the occurrence of side effects such as inflammation, scarring, and functional impairments in the irradiated area. An equally important aspect of this problem is the impracticability to deliver radiation doses sufficient for radical treatment, which, in turn, necessitates additional fractionation of radiotherapy sessions [1, 2], thereby increasing the burden on medical personnel and equipment as well as on patients.

Therefore, a relevant task is to develop new methods to enhance the efficiency of converting the energy of therapeutic X-ray beams within a targeted region of the body. One promising approach to increase tumor contrast involves introducing high atomic number nanoparticles into the specified volume [3, 4]. The increased probability of interactions between metals and photons, relative to biological tissue, results in a higher number of interaction events between nanoparticles and radiation. In its turn, induced secondary radiation creates an additional dose component in the vicinity of the nanoparticle, thereby amplifying its destructive effect on the tumor. The short mean free path characteristic of X-ray-induced secondary radiation ensures that these effects are localized, reducing the risks of overexposure to non-targeted organs and tissues.

This work aims to investigate the features of irradiation of composite Fe_3O_4-SiO_2-Au nanoparticles, specifically focusing on determining how the size and number of gold nanoparticles on the surface of Fe_3O_4-SiO_2 influence the yield of secondary radiation emitted from nanoparticle surfaces.

Materials and Methods

The nanoparticle model was based on data from real systems with a “core-shell-satellite” structure: a magnetite core coated with a thin film of amino silica, onto which gold nanoparticles are attached [5]. The systems are presented in two configurations which differ in the nanoparticle coverage density on the surface of the SiO_2 adhesion layer. The average number of GNP per Fe_3O_4-SiO_2 nanoparticle was 16 ± 4 for the first system and 40 ± 12 for the second. The average size of the iron-containing core was 62 ± 10 nm for both systems. The size of the gold nanoparticles (GNP) on the adhesive layer surface was 13.7 ± 1.9 nm and 9.5 ± 1.8 nm for the first and second systems, respectively [5].

A series of numerical experiments was performed to identify the features of X-ray irradiation of the described nanoparticles. A more detailed description of the simulation model, creation method, and calculation methodology is presented in our previous work [5]. Here are the key parameters.

The simulation of radiation transfer processes was performed using the general-purpose radiation transport Monte Carlo code PHITS version 3.33 [6–9]. In this work, the track-structure mode was utilized in all geometric areas for particles with energies ranging from 100 eV to 10 keV. For interactions involving particles with energies higher than 10 keV, the EGS5 (Electron-Gamma Shower) code was used as part of PHITS.

Table 1

Geometric parameters of targets and model comparison

	This work				A system equivalent in chemical composition [5]			
	$d[Fe_3O_4]$, nm	$\tau[SiO_2]$, nm	d[Au], nm	n[Au]	$d[Fe_3O_4]$, nm	$\tau[SiO_2]$, nm	d[Au], nm	n[Au]
Set1	87	2	10	31	87	2	5	331
Set2	87	2	10	62	87	2	5	661
Set3	87	2	10	208	87	2	5**	–

Notations: $d[Fe_3O_4]$, d[Au] – diameter of Fe_3O_4 core and Au nanoparticles; $\tau[SiO_2]$ – thickness of SiO_2 adhesive layer; n[Au] – the number of Au nanoparticles on SiO_2 adhesive layer.
**The adhesive layer was coated with a continuous layer (shell) of Au with a thickness of 5 nm.

An approach based on a spherical Fibonacci lattice was used to implement a physical model of the experimentally obtained core-shell nanoparticles [10]. Such approach allows to achieve uniform distribution of gold nanoparticles on the surface of adhesion layer of SiO_2. The coordinates of the AuNPs on the SiO_2 shell surface were defined in the geometry for PHITS simulations using the FitsGeo code [11]. This study considered four configurations of core-shell-satellite geometry. The targets parameters are demonstrated in Table 1.

The target was irradiated with a parallel monoenergetic X-ray beam. The photon energy was 50, 100, and 150 keV. At each independent simulation, 108 primaries were transported to provide good statistics. The flat circular radiation source was positioned so that its axis coincided with the centre of the nanoparticle. The diameter of the source coincided with that of the nanoparticle. The source was placed close to the nanoparticle.

We considered the physical processes responsible for electron generation and the spectra of secondary electrons crossing the sphere that encloses the target. To account for changes in the geometric parameters of the radiation source and detectors (their area) relative to similar parameters used in previous work [5], data on the particle flux crossing the sphere was renormalized.

Results and Discussion

At the first stage, the spectra of secondary electrons emitted from the target surface were analyzed. The overall shape of the spectra for a system with large gold nanoparticles (10 nm) is similar to that recorded from the surface of previously analyzed systems with smaller nanoparticles (5 nm) [5]. To assess the effect of nanoparticle size, the obtained spectra were conventionally divided into several regions: the Auger electron region (6–10 keV), and the photoelectron regions at 30–40 keV, 70–95 keV, and 80–120 keV for primary beam energies of 50, 100, and 150 keV, respectively, corresponding to emissions from iron and gold. The electron fluences within each of these energy ranges were summed. The intensity of electron emission for systems with different nanoparticle sizes but identical gold content is comparable across all energy ranges, regardless of the primary photon energy. The data indicates the absence of self-shielding effects as particle size increases for high-energy (>1 keV) electrons.

A significant reduction in secondary electron emission with an increase in the GNPs size in the system was recorded in the low energy region (< 1 keV) of the spectrum (Table 2). A dependence of this effect on the density of the GNPs coverage was also identified. Let Φ_5 and Φ_{11} be the flux of secondary electrons with kinetic energy <1 keV for systems with a GNPs diameter of 5 and 11 nm, respectively. The ratio Φ_{11}/Φ_5 increases with an increase in the surface concentration of GNP on the SiO_2 shell.

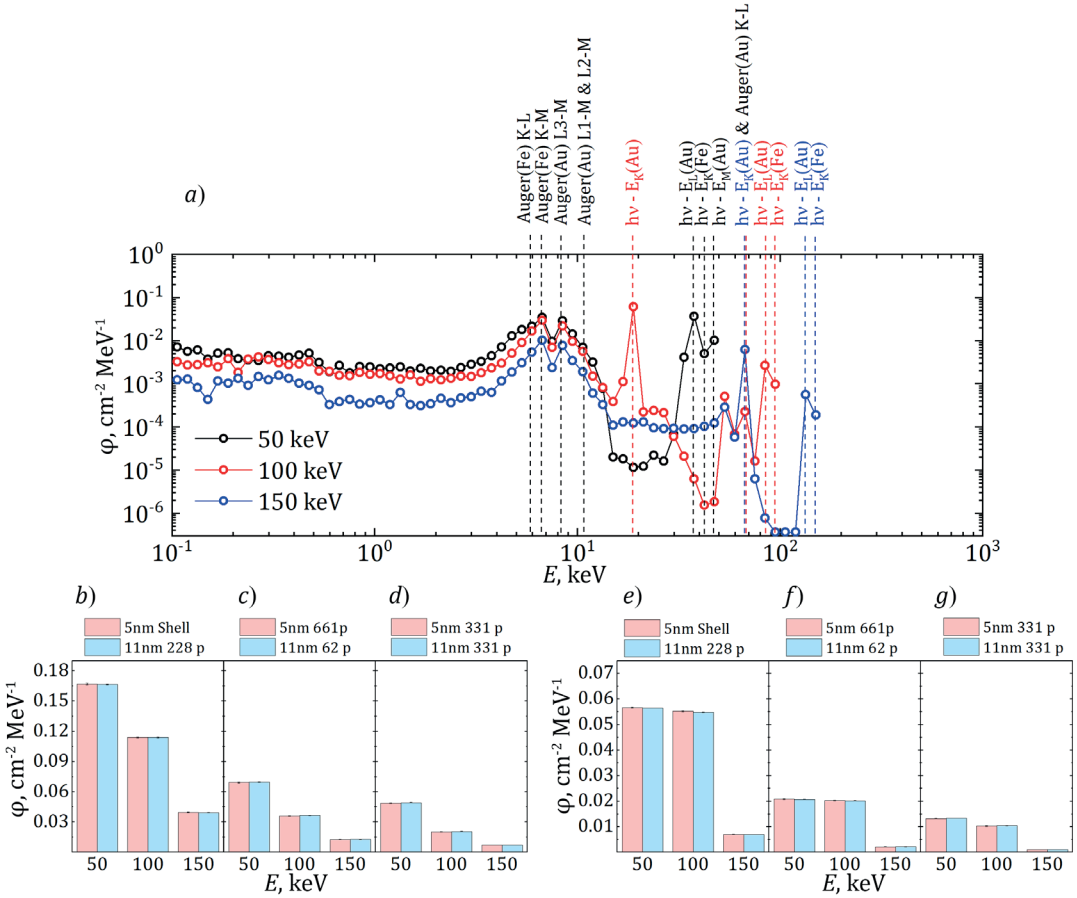

Fig. 1 Simulated spectra of secondary electrons emitted from the target (for example, 11nm 228p system) surface during its irradiation by photons with different energy (where K-L, K-M, L3-M, L2-M, and L1-M indicate the energy differences between the corresponding electron shells of atoms) (*a*); comparison of the emission intensity of Auger electrons (*b*, *c*, *d*) and photoelectrons (*e*, *f*, *g*) from the target surface for 50, 100, and 150 keV photons respectively

Table 2

Geometric parameters of targets and model comparison

	Φ_5, $cm^{-2}\ MeV^{-1}$	$\Phi_{11}\cdot10^{-3}$, $cm^{-2}\ MeV^{-1}$	Φ_{11}/Φ_5	$V_{Water\_5}\cdot10^{-3}$, nm^3	$V_{Water\_11}\cdot10^{-3}$, nm^3	Φ_{11}/Φ_5
*Set1	4.61 (5.5)	2.99 (4.2)	0.648 (4.3)	123.2	339.2	0.363
*Set2	5.19 (6.7)	3.57 (3.8)	0.688 (3.8)	101.5	318.3	0.319
*Set3	8.25 (4.2)	8.12 (2.5)	0.985 (2.5)	0	215.9	0

Notations: *Set1-3 corresponds to the numbering in Table 1.
The relative error in determining the parameters is given in parentheses.

The increase in electron emission with increasing of GNP lattice density can be attributed to a decrease in electron path length into the aqueous medium. In rarefied systems, the mean path length of secondary electrons passes through the water-filled volume between the GNPs and the detector increases. This leads to lower measurement results. This hypothesis is confirmed by the value of the Pearson coefficient $R = 1$ for the dependence $\Phi_{11}/\Phi_5 = f(V_{Water\_11} / V_{Water\_5})$, where V_{Water_11} and V_{Water_5} – is the volume of water filling the space between the GNP and the bounding sphere (electron detector) for systems with a GNP size of 5 and 11 nm, respectively.

Conclusion

PHITS calculations revealed that the emission intensity of secondary electrons with energies above 1 keV from Fe_3O_4–SiO_2–Au nanoparticles is independent of the size of the gold nanoparticles, given their uniform distribution on the adhesive layer. The stability of the secondary electron emission intensity with energy >1 keV is because the average thickness of the gold layer that an electron must pass does not exceed its mean free path in gold [12]. A decrease in emission intensity was observed in the low energy region of the spectrum ($E < 1$ keV). This effect is attributed to the model parameters, specifically the absorption of electrons in the water filling the volume between the GNPs. The presence of this effect precludes a definitive conclusion regarding the presence or absence of effects associated with the self-shielding of electron of this energy group. In the future, it is planned to replace the interparticle medium with a vacuum.

The main factors controlling the configuration of dose fields are the chemical composition of the nanoparticles and the energy of the primary photon beam.

REFERENCES

1. **Kaanders J.H., Ang K.K.,** Early reactions as dose-limiting factors in radiotherapy, Seminars in radiation oncology. 4 (2) (1994) 55–67.

2. **Gaya A.M., Ashford R.F.U.,** Cardiac complications of radiation therapy, Clinical oncology. 17(3) (2005) 153–159.

3. **Siddique S., Chow J.C.L.,** Application of nanomaterials in biomedical imaging and cancer therapy, Nanomaterials. 10 (9) (2020) 1700.

4. **Song G., Cheng L., Chao Y., Yang K., Liu Z.,** Emerging nanotechnology and advanced materials for cancer radiation therapy, Advanced materials 29 (32) (2017) 1700996.

5. **Markin N.S., Gordeev I.S., Fu H.E., Ivannikov S.I., Kim Y.B., Samardak A.Y., Samardak A.S., Kim Y.K., Ognev A.V.,** Secondary electron dynamics in core–shell–satellite nanoparticles: a computational strategy for targeted cancer treatment, Nanoscale. 17 (18) (2025) 11691–11702.

6. **Sato T., Iwamoto Y., Hashimoto S., Ogawa T., Furuta T., Abe S.-I., Kai T., Matsuya Y., Matsuda N., Hirata Y., Sekikawa T., Yao L., Tsai P.-E., Ratliff H.N., Iwase H., Sakaki Y., Sugihara K., Shigyo N., Sihver L., Niita K.,** Recent improvements of the particle and heavy ion transport code system–PHITS version 3.33, Journal of Nuclear Science and Technology. 61 (1) (2024) 127–135.

7. **Sato T., Iwamoto Y., Hashimoto S., Ogawa T., Furuta T., Abe S.-I., Kai T., Tsai P.-E., Matsuda N., Iwase H., Shigyo N., Sihver L., Niita K.,** Features of particle and heavy ion transport code system (PHITS) version 3.02, Journal of Nuclear Science and Technology. 55 (6) (2018) 684–690.

8. **Hirayama H., Namito Y., Nelson W.R., Bielajew A.F., Wilderman S.J.,** The EGS5 Code System, Department of Energy Stanford University: Stanford, CA, USA. (SLAC-R-730). (2005).

9. **Kai T., Yokoya A., Ukai M., Fujii K., Watanabe R.,** Thermal equilibrium and prehydration processes of electrons injected into liquid water calculated by dynamic Monte Carlo method, Radiation Physics and Chemistry. 115 (2015) 1–5.

10. **González Á.,** Measurement of areas on a sphere using Fibonacci and latitude–longitude lattices, Mathematical geosciences. 42 (2010) 49–64.

11. **Gordeev I.,** FitsGeo – Python package for PHITS geometry development and visualization, arXiv preprint arXiv:2008. 03298 (2020).

12. **Chaynikov A.P., Kochur A.G., Dudenko A.I.,** Simulation of energy absorption processes in water near the surface of gold nanoparticle under X-ray photon irradiation, Journal of Experimental and Theoretical Physics. 166 (2) (2024) 194–208.

THE AUTHORS

MARKIN Nikita S.
markkin.ns@gmail.com
ORCID: 0000-0001-8974-2235

GORDEEV Ivan S.
gordeev@jinr.ru
ORCID: 0000-0003-3120-3401

IVANNIKOV Sergey I.
fyajkfqn@mail.ru
ORCID: 0000-0002-5889-3409

SAMARDAK Aleksei Yu.
samardak.aiu@dvfu.ru
ORCID: 0000-0002-0795-374X

SAMARDAK Alexander S.
samardak.as@dvfu.ru
ORCID: 0000-0001-5917-4361

OGNEV Alexey V.
ognev.av@dvfu.ru
ORCID: 0000-0002-1619-3666

Received 11.09.2025. Approved after reviewing 25.09.2025. Accepted 29.09.2025.